Highly reactive Cu-Pt bimetallic 3D-electrocatalyst for selective nitrate reduction to ammonia

Gabriel Antonio Cerrón-Calle, Ana S. Fajardo, Carlos M. Sánchez-Sánchez, Sergi Garcia-Segura

PII: S0926-3373(21)00969-3

DOI: https://doi.org/10.1016/j.apcatb.2021.120844

Reference: APCATB120844

To appear in: *Applied Catalysis B: Environmental*

Received date: 21 July 2021
Revised date: 22 October 2021
Accepted date: 22 October 2021

Please cite this article as: Gabriel Antonio Cerrón-Calle, Ana S. Fajardo, Carlos M. Sánchez-Sánchez and Sergi Garcia-Segura, Highly reactive Cu-Pt bimetallic 3D-electrocatalyst for selective nitrate reduction to ammonia, *Applied Catalysis B: Environmental,* (2021) doi:https://doi.org/10.1016/j.apcatb.2021.120844

Highly reactive Cu-Pt bimetallic 3D-electrocatalyst for selective nitrate reduction to ammonia

Gabriel Antonio Cerrón-Calle[a], Ana S. Fajardo[a,b,*], Carlos M. Sánchez-Sánchez[b], Sergi Garcia-Segura[a,**]

[a]Nanosystems Engineering Research Center for Nanotechnology-Enabled Water Treatment, School of Sustainable Engineering and the Built Environment, Arizona State University, Tempe, AZ 85287-3005, USA

[b]Sorbonne Université, CNRS, Laboratoire Interfaces et Systèmes Electrochimiques (LISE), 4 place Jussieu, F-75005, Paris, France

Article submitted to be published in

Applied Catalysis B: Environmental

Corresponding author:

*e-mail: adossan3@asu.edu (Dr. Ana Sofia Fajardo)

**e-mail: Sergio.garcia.segura@asu.edu (Dr. Sergi Garcia-Segura)

Abstract

Identifying electrocatalytic materials that generate fossil-free ammonia through N-recycling from polluted water sources is required. Bimetallic Cu-Pt foam electrodes were synthesized to enhance electrochemical reduction of nitrate (ERN) by the introduction of bimetallic catalytic sites. Electrodes were benchmarked against Cu foam using engineering figures of merit. Cu-Pt (180 s) electrode achieved 94% conversion of NO_3^--N in 120 min yielding 194.4 mg NH_3- N L^{-1} g_{cat}^{-1}, with a selectivity towards ammonia (S_{NH_3}) of 84% and an electrical energy per order decrease by ~70% respect pristine Cu foam. Bimetallic electrodes with low Pt loadings (<0.50 wt%) demonstrated that synergistic effects of Cu-Pt nanointerfaces enabled hybridized mechanisms of catalytic electrochemical and hydrogenation reduction processes. These encouraging outcomes emphasize the potential of Cu-Pt foam electrodes to treat contaminated water sources with nitrate, while allowing a sustainable decentralized ammonia recovery. Enriched water for crops irrigation can therefore be a prospect use for this added value product.

Keywords: water treatment, selective electrocatalytic reduction, resource recovery, denitrification, ammonia production

1. Introduction

The exponential growth of the world population has pushed scientists to develop chemical substances to increase crop yield and ensure food production. Ammonia is key in most crop fertilizer formulations that are essential to secure global food supply [1]. Despite the undeniable benefits of ammonia production, indirect hazardous effects related to ammonia usage causes serious environmental problems related to the anthropogenic disruption of the natural nitrogen cycle [2]. Artificial nitrogen fixation has contributed to the buildup of nitrogen species in the biosphere. Ammonia leached into ground and surface waters is easily transformed in the environment via biotic and abiotic processes to nitrate. Nitrate pollution in waters is due to anthropogenic activities including, but not limited, to fertilizer runoff from crops, animal farming, and industrial wastewater [3–5]. Nitrate is considered one of the top 10 drinking water pollutants above the maximum contamination level (MCL > 10 mg NO_3^--L^{-1}) not only in the US, but worldwide [10,11]. High concentrations of this contaminant pose alarming risks to human health, as they trigger cancer, thyroid problems, and adverse respiratory effects [12–15].Therefore, there is a pressing need to reduce nitrate from water streams. This approach is also an unexploited source of nitrogen that could be used for decentralized ammonia production at ambient conditions for agricultural use with a significantly lower cost [8,9]. Decentralized production of ammonia in rural areas can minimize environmental impacts of Haber-Bosch process (including produced ammonia distribution), while remediating polluted water sources by artificially reinstating the nitrogen cycle. Electrocatalytic processes, by operating at ambient conditions, being compact and easy to handle, are emerging as encouraging sustainable alternative technology.

The electrochemical reduction of nitrate (ERN) can selectively reduce nitrate to ammonia (Eq. 1). The ERN presents itself as a step up to the classical N_2 electrochemical reduction (the direct electrocatalytic alternative of Haber-Bosch) which suffers from the challenging protonation and splitting of the N≡N triple-bond [16–20]. Sustainable ERN from polluted water sources holds the potential to enable fossil-free ammonia production through N-recycling approaches when operated with renewable energy sources.

$$NO_3^- + 9H^+ + 8e^- \rightarrow NH_3 + 3H_2O \quad (1)$$

The study of the ERN applied to ammonia production it is still in an early stage [21–23]. According to the literature [24], mass transport limitations must be overcome to increase the performance of the process. Three-dimensional (3D) electrodes, due to their porous structure can increase the specific surface area, allowing a higher catalytic reduction of pollutants [25]. In this context, copper (Cu) foam has been reported as one of the materials with the best kinetics for the nitrate reduction limiting step (Eq. 2) which is associated to the first charge transfer from nitrate to nitrite [26]. The initial reduction of nitrate towards nitrite is a three-step electrochemical-chemical-electrochemical (ECE) mechanism as described in reactions (2) – (4).

$$NO_{3\,(ads)}^- + e^- \longrightarrow NO_{3\,(ads)}^{2-} \qquad \textit{limiting step} \quad (2)$$

$$NO_{3\,(ads)}^{2-} + H_2O \longrightarrow NO_{2\,(ads)}^{\bullet} + 2OH^- \quad (3)$$

$$NO_{2\,(ads)}^{\bullet} + e^- \longrightarrow NO_{2\,(ads)}^- \quad (4)$$

Copper, being a metal with highly occupied d-orbitals and due to the similarity between its energy level and the lowest unoccupied molecular π* orbital of nitrate [24], enables a smooth and fast reduction of nitrate to nitrite. However, copper-based catalysts by themselves may decrease contaminant removal efficiency over time since are easily deactivated or corroded. To improve the reactivity of the electrodes, bimetallic catalysts are being developed by coating small amounts of a transition (*e.g.*, Cu, Fe, Ni, Mo) or noble metals (*i.e.*, Pd, Pt) onto a metallic substrate [8,27]. Bimetallic catalysts hold the promise of enhancing activity, selectivity, and stability of the electrode due to synergistic interactions between both metal components. Nano-decoration of a macro metallic material is a barely explored approach that can benefit from bimetallic nanointerfaces conjugation. Existence of nano-interfacial domains can modify the adsorption characteristics of the bimetallic catalyst's surface and, in some cases, even alter its selectivity towards a specific by-product. The aim of this research is to enhance catalytic performance of ERN and the selectivity towards ammonia production. During the ERN in aqueous media, water reduction to stable adsorbed hydrogen ($H_{(ads)}$, Eq. 5) has been considered as a competitive coexisting reaction, being

especially relevant on noble metals such as Pt and Pd [28]. However, the stabilization of $H_{(ads)}$ as strong reductant on certain metallic surfaces can facilitate indirect electrochemical reduction processes. Contribution of hydrogenation mechanisms to ERN cannot be disregarded due to the strong reducing environment created by the presence of $H_{(ads)}$. Consecutive reactions between the formed nitrogen intermediate species and $H_{(ads)}$ have been reported to potentially lead to ammonia production in catalytic hydrogenation (Eqs 6 - 11).

$$H_2O + e^- \longrightarrow H_{(ads)} + OH^- \quad (5)$$

$$NO_{3\,(ads)}^- + 2H_{(ads)} \longrightarrow NO_{2\,(ads)}^- + H_2O \quad (6)$$

$$NO_{2\,(ads)}^- + H_{(ads)} \longrightarrow NO_{(ads)} + OH^- \quad (7)$$

$$NO_{(ads)} + 2H_{(ads)} \longrightarrow N_{(ads)} + H_2O \quad (8)$$

$$N_{(ads)} + H_{(ads)} \longrightarrow NH_{(ads)} \quad (9)$$

$$NH_{(ads)} + H_{(ads)} \longrightarrow NH_{2\,(ads)} \quad (10)$$

$$NH_{2\,(ads)} + H_{(ads)} \longrightarrow NH_{3\,(ads)} \quad (11)$$

Platinum is a metallic material, which has already demonstrated satisfactory performance as electrocatalyst for different electrochemical processes such as O_2 reduction [29], formic acid and CO oxidations [30–32] as well as hydrogenation [33,34]. It is well known that Pt particles cannot hydrogenate nitrate but present excellent kinetic rates for nitrite reduction towards ammonia [35,36]. Most studies on bimetallic electrocatalysts using Pt-Cu consist of platinum nanoparticles coated with copper that are deposited onto conductive substrates (e.g., glassy carbon) through the drop-casting of inks containing usually a perfluorinated ionomer (i.e., nafion) which given the raising concerns regarding perfluoroalkyl substances (PFAS) may not be the most suitable material choice when treating water for environmental remediation. Drop-casted electrodes show low-stability since the deposited nanoparticles easily wear-off if they face hydrodynamic conditions in large scale flow cells intended to treat large volumes of water.

In contrast, the objective of the research presented herein was to develop bimetallic electrodes by electrodepositing small loads of Pt (< 0.50 wt%) nanoparticles on the surface of a copper foam substrate

to enhance the ERN and boost the electrogeneration of ammonia. Electrodeposition of Pt on bulk copper electrode can minimize the use of platinum forming bimetallic nanodomains while providing a more robust attachment than drop-casted nanoparticles. Under identical initial pH and nitrate concentration conditions, Cu and Cu-Pt foam electrodes were benchmarked in terms of nitrate conversion figures of merit and product selectivity. Electrical energy per order (EE/O) and the Faradaic efficiency (FE) were calculated to discuss about the competitiveness of the new synthesized electrodes for ammonia generation and to evaluate the prospective opportunities for the translation of the ERN system to a higher technology readiness level.

2. Materials and methods

2.1 Chemicals and materials

Reagent grade acetone, hydrochloric acid, potassium tetrachlroroplatinate, sodium nitrate, sodium nitrite, and ammonia sulfate (>99%) were purchased from Sigma-Aldrich. Analytical-grade sodium sulfate (99%, Sigma-Aldrich) was used as the supporting electrolyte. Copper foam of 99.99% purity with 110 pore per inch supplied by Futt was used as an electrode substrate. All solutions were prepared with ultrapure water with resistivity >18.2 MΩ cm at 25 °C (Millipore Milli-Q system).

2.2. Electrodeposition of Pt over Cu substrate

The electrodeposition of Pt on Cu material was performed using a potentiostat (PGSTAT302N, Metrohm. USA) under potentiostatic conditions. A three-electrode system was set up using an Ag/AgCl as the reference electrode, a 5 cm^2 stainless-steel plate as auxiliary electrode, and copper foam with a 2.25 cm^2 geometrical area as the working electrode. Before use, the copper foam was washed in acetone using ultrasonic bath during 30 min, rinsed with 0.1 mol L^{-1} HCl, then thoroughly cleaned with ultrapure water and dried at room temperature. The electrodeposition of platinum on copper was conducted using chronoamperometry under continuous cathodic potential of -0.15 V vs Ag/AgCl (3 mol L^{-1} KCl) for different times 60 s, 120 s, 180 s, and 360 s. The different nano-composite electrodes were identified by

the time of electrodeposition as Cu-Pt 60 s, Cu-Pt 120 s, Cu-Pt 180 s, and Cu-Pt 360 s. The electrodeposition bath consisted of a solution of 3 mmol L^{-1} K_2PtCl_4 dissolved in 0.5 mol L^{-1} H_2SO_4 [37]. Electrosynthesized nanocomposite Cu-Pt electrodes were rinsed with ultrapure water and dried at room temperature. Dried Cu-foam electrodes were weighted prior and after electrodeposition. The theoretical amount of total Pt deposited on Cu foam were (~0.30 wt%, ~0.33 wt%, ~0.36 wt%, ~0.47 wt% electrodeposited at 60 s, 120 s, 180 s and 360 s, respectively. The increment of electroactive surface was proved by specific capacitance (F g^{-1}) evaluated in 0.1 mol L^{-1} Na_2SO_4 as presented by Zhu and Zhao [38].

2.3. Three-dimensional electrode characterization

The morphology difference of Cu foam and Cu-Pt electrodes was characterized by scanning electron microscope using a Nova 200 Nanolab at 5 kV and 1.6 nA. Energy-dispersive X-ray spectroscopy (EDS) was performed using an ESEM-FEG XL30 at 15 kV for *in situ* elemental mapping of the Cu-Pt electrodes. Crystallographic composition of the electrodes was evaluated by X-ray diffraction (XRD) using a PANanalytical Aeris Powder by applying Cu $K_{\alpha 1+2}$ radiation ($\lambda_{(\alpha 1)}$ = 0.154060 nm) at 40 kV and 20 mA current. The oxidation states of copper were evaluated by X-ray photoelectron spectroscopy (XPS) was measured by VG 220i-XL with X-Ray source monochromate Al K-alpha with a line width of 0.7 eV.

2.4. Electrochemical characterization of three-dimensional electrodes

Electroanalytical characterization of Cu and Cu-Pt electrodes was carried out by cyclic voltammetry (CV) and linear sweep voltammetry (LSV) in a conventional three electrode system. The electrochemical cell employed the three-dimensional foam (nano-enabled or not) as working electrode, a stainless-steel plate as auxiliary electrode, and an Ag/AgCl as the reference electrode. All reported potentials are referenced to reversible hydrogen electrode (RHE), using the Eq. (12).

$$E(RHE) = E_{Ag/AgCl} + 0.059\,pH + E^{\circ}_{Ag/AgCl} \quad (12)$$

where $E°_{Ag/AgCl}$ is 197 mV at 25 °C. The volume of Cu foam electrodes was 1.5 cm x 1.5 cm x 0.2 cm, and all electrochemical measurement were normalized using the electrode geometrical area (cm^2). The electrocatalytic response for direct charge transfer ERN was studied by CV at 10 mV s^{-1} in solutions of 0.1 mol L^{-1} Na_2SO_4 as support electrolyte in presence or absence of nitrate ion (10 mmol L^{-1} $NaNO_3$). The solutions were initially purged with N_2. Additional voltametric analyses were conducted in presence of nitrite ion (10 mmol L^{-1} $NaNO_2$) allowing reduction peaks identification.

2.5. Electrochemical reduction of nitrate

Electrochemical reduction experiments were conducted galvanostatically at 0.09 A (TENMA 72-2720 DC power supply) in an open, undivided cylindrical glass batch reactor containing 100 mL of non-deaerated 30 mg NO_3^--N L^{-1} solutions with 12.5 mmol L^{-1} Na_2SO_4 (pH = 6.27±0.01 and conductivity = 3.04±0.05 mS cm^{-1}) at 25 °C. This model solution mimics the nitrate concentration (mg NO_3^--N L^{-1}) typically found in a groundwater containing nitrate over maximum concentration levels. The electrochemical set-up was equipped with two parallel electrodes (geometrical area 1.5 cm × 1.5 cm) with an interelectrode gap distance of 1.0 cm. The pristine Cu foam or Pt nano-enabled Cu foams were used as cathode, while a commercial Ti/IrO_2 (DeNora – USA) was used as anode. Batch reactor experiments were continuously mixed using magnetic stirring at 500 rpm to ensure transport from/towards the electrode surface. Samples were withdrawn over time and analyzed for nitrogenous species (NO_3^--N, NO_2^--N and NH_3-N), conductivity, and pH. Experiments were run in triplicate, and deviations between them were lower than 5% for all trials.

To understand the role of N-species re-oxidation back to nitrate, control experiments were performed using initial solutions of 30 mg L^{-1} NO_2^--N or 30 mg L^{-1} NH_3-N solutions with 12.5 mmol L^{-1} Na_2SO_4. According to Fig. SM1, it was verified that no oxidation of nitrite or ammonia to nitrate occurred.

2.6. Analytical instruments and procedures

The pH and conductivity were measured using Thermo Scientific Orion Star A221 meters. Nitrate, nitrite, and ammonia were quantified with a HACH DR6000 UV-vis equipment using TNT 835, TNT 839 and TNT 830 HACH kits, respectively. Nitrate conversion was calculated using Eq. (13).

$$Nitrate\ conversion\ (\%) = \frac{C_{nitrate,i} - C_{nitrate,t}}{C_{nitrate,i}} \times 100 \quad (13)$$

where $C_{nitrate,i}$ is the nitrate concentration in mg NO_3^--N L^{-1} before treatment, and $C_{nitrate,t}$ is the nitrate concentration at time (*t*). A mass balance on aqueous nitrogen species led to the determination of the N-volatile species (N_2, NO, NO_2 or N_2O). Previous literature suggests that N-volatiles are mostly associated to innocuous N_2 evolution [39]. The possibility of ammonia volatilization was disregarded from the blank experiments shown in Fig. SM1b, since the content of ammonia remained constant throughout the entire blank experiment.

The selectivity (S_X) towards ammonia was calculated using Eq. (14).

$$S_{NH_3}(\%) = \frac{C_{ammonia}}{C_{nitrate,i} - C_{nitrate,t}} \times 100 \quad (14)$$

where $C_{ammonia}$ represents the concentration of ammonia (mg NH_3-N L^{-1}), produced over time.

Faradaic efficiency (FE, Eq. (15)) was used as figure of merit that determines system performance from the number of electrons consumed in an electrochemical reaction relative to the expected theoretical conversion ruled by Faraday's law.

$$FE(\%) = \frac{n\ F\ N_i}{3600\ I\ t} \times 100 \quad (15)$$

where *n* is the number of electrons required per mol of ammonia (mol), *F* is the Faraday constant (96 485 C mol^{-1}), N_i is the mol of ammonia generated during the electrolysis, *I* is the applied electric current (A), *t* is the electrolysis time (h), and 3600 is a unit conversion factor (3600 s h^{-1}).

Electrical energy per order (*EE/O)*, was used as an engineering figure of merit to benchmark the electric energy required to reduce NO_3^--N concentration by one order of magnitude in a unit volume calculated from Eq. (16) for batch operation mode.

$$EE/O\ (kWh\,m^{-3}order^{-1}) = \frac{E_{cell}It}{V_s log(C_0/C_t)} \quad (16)$$

where E_{cell} is the average of the cell potential (V), I is current intensity (A), t is time (h), V_s is solution volume (L), and C_0 and C_t are the initial and final concentrations of nitrate. Considering the relationship $\log(C_0/C_t) = 0.4343 \bullet t \bullet k_1$, the *EE/O* expression can be simplified assuming first-order kinetics according to Eq. (17) where 6.39×10^{-4} is a conversion factor:

$$EE/O\ (kWh\,m^{-3}order^{-1}) = \frac{6.39 \times 10^{-4} E_{cell} I}{V_s k_1} \quad (17)$$

Inductively coupled plasma mass spectrometry (ICP-MS), using Perkin Elmer Nexion 1000, was recorded for the solution sample obtained after the electrolysis using the cathode Cu-Pt 180 s to find Cu and Pt leaching. The sample was measured in triplicate using a dual detector.

3. Results and discussion

3.1. Characterizing three-dimensional copper foams nano-enabled with platinum

The electrodeposition of platinum over copper foam induced *in-situ* growth of nanoparticles that form bimetallic catalytic sites. The XRD analyses were carried out to identify the crystallographic structure of the nano-composite bimetallic electrode. Fig.1a shows peaks of the cubic structure of pure Cu phase (JCPDS N° 003-1018) at 43.2, 50.3, and 74.0 ° corresponding to the planes (111), (200), and (220), respectively. The peaks at 29.0, and 48.0 ° were attributed to the planes (110) and (111) of Cu_2O cubic structure (JCPDS N° 05-0667). The small peak at 47.1 ° corresponded to the plane (200) of face centered cubic structure of pure Pt phase (JCPDS N° 04-0802). Platinum peak increased with the deposition time due to the higher content of Pt. Note that for electrodes with lower than 0.50 wt% compositions of Pt, diffraction peaks of Pt domains were not observed as commonly reported in literature for lower contents in nanocomposite materials. These results suggest that independent Pt domains are formed pointing to the obtaining of a bi-metallic nanocomposite.

The oxidation state of copper in Cu foam and Cu-Pt electrode was studied by using XPS. The XPS spectrum of Cu 2p in Cu foam (Fig. 1b) presents the peaks at 932 eV and 951 eV which can be assigned to Cu(0) and/or Cu(I) due to the separation between Cu(0) and Cu(I) that is about 0.3 eV. The small peaks at 935 eV and 954 eV indicate the Cu(II) oxidation state, forming copper oxide (II). Remarkable is the higher intensity peaks at 933 and 954 eV associated to Cu 2p observed in Cu-Pt electrodes (Fig. 1c) that indicates more Cu(II) is present than within the pristine Cu foam. The wide XPS spectrum of Cu-Pt electrode (Fig. 1d) reveals Pt at 76.0 eV. However, due to low amount of this element (0.50 wt%), the XPS cannot identify the oxidation state.

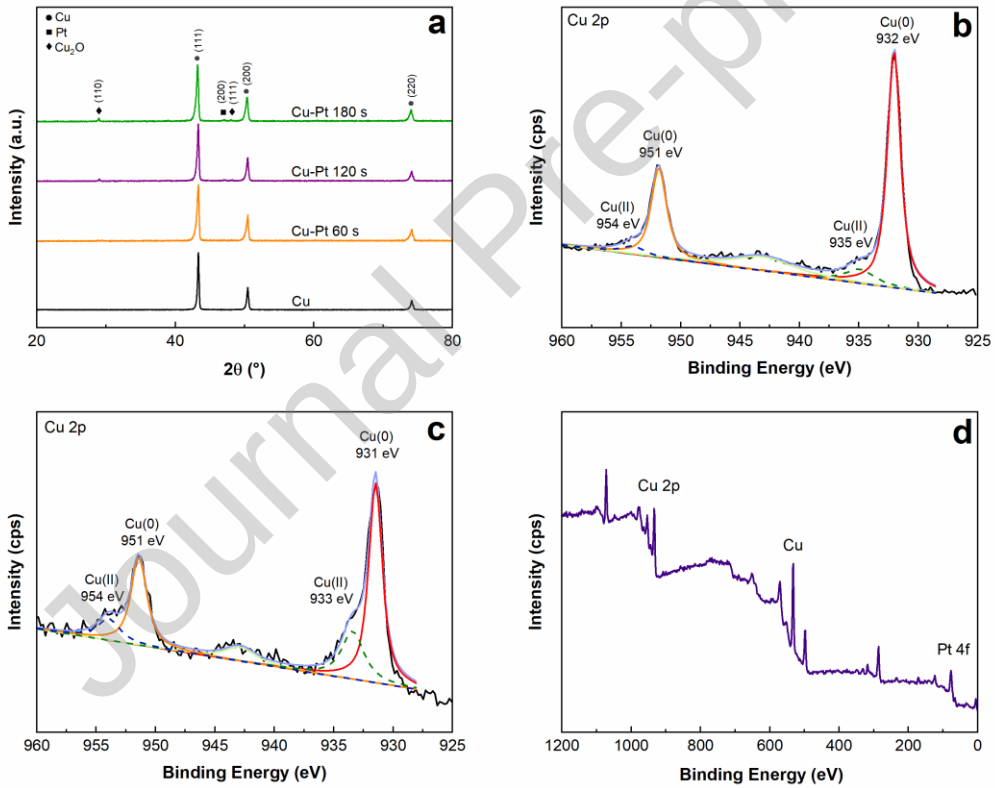

Figure 1. (a) XRD patterns of the Cu foam and Cu-Pt at different times of electrodeposition. (b) XPS spectra of Cu 2p in copper foam, (c) XPS spectra of Cu 2p in Cu-Pt 180 s electrode, and (d) Wide scan XPS spectra for Cu-Pt electrode.

The morphology of Cu foam and Cu-Pt electrodes is illustrated at different magnifications (65x, 8000x 50000x) by SEM in Fig. 2. At 65x (Fig. 2a), The Cu foam exhibited a 3D framework with macro-porous as can be seen in Fig. 2a at 65x. Higher magnification (8000x, Fig. 2b) allowed to verify the smooth surface of pristine Cu foam. Conversely, Cu-Pt electrodes (Fig. 2c-e) show the presence of nanoparticles attached to the copper surface. The average size and amount of platinum nanoparticles increased with the electrodeposition time. The average size of the nanoparticles was 150 ± 20 nm for Cu-Pt 60 s, 180 ± 40 nm for Cu-Pt 120 s, and 280 ± 50 nm for Cu-Pt 180 s. Longer deposition times promote crystal growth over nucleation of Pt domains on the Cu foam, for this reason Cu-Pt 60 s (Fig. 2c) presents more monodispersed particles than Cu-Pt 120 s (Fig. 2d) or Cu-Pt 180 s (Fig. 2e). For higher times than 60 s the copper foam surface was coated with Pt nanoparticles and some particles growth and differentiate from the background. Note that higher deposition times promoted formation of bigger clusters of platinum (Fig. SM2) that can decrease availability of Cu-Pt bimetallic sites given the increase on the surface of homogeneous Pt domains. The elemental composition at the surface of the electrodes was obtained by EDS and it is summarized in Table 1. The amount of platinum increased with higher depositions from around 6 to 17 wt%, and the small amount of oxygen (1 - 6 wt%) might correspond to Cu_2O and CuO in agreement with the XRD and XPS analyses.

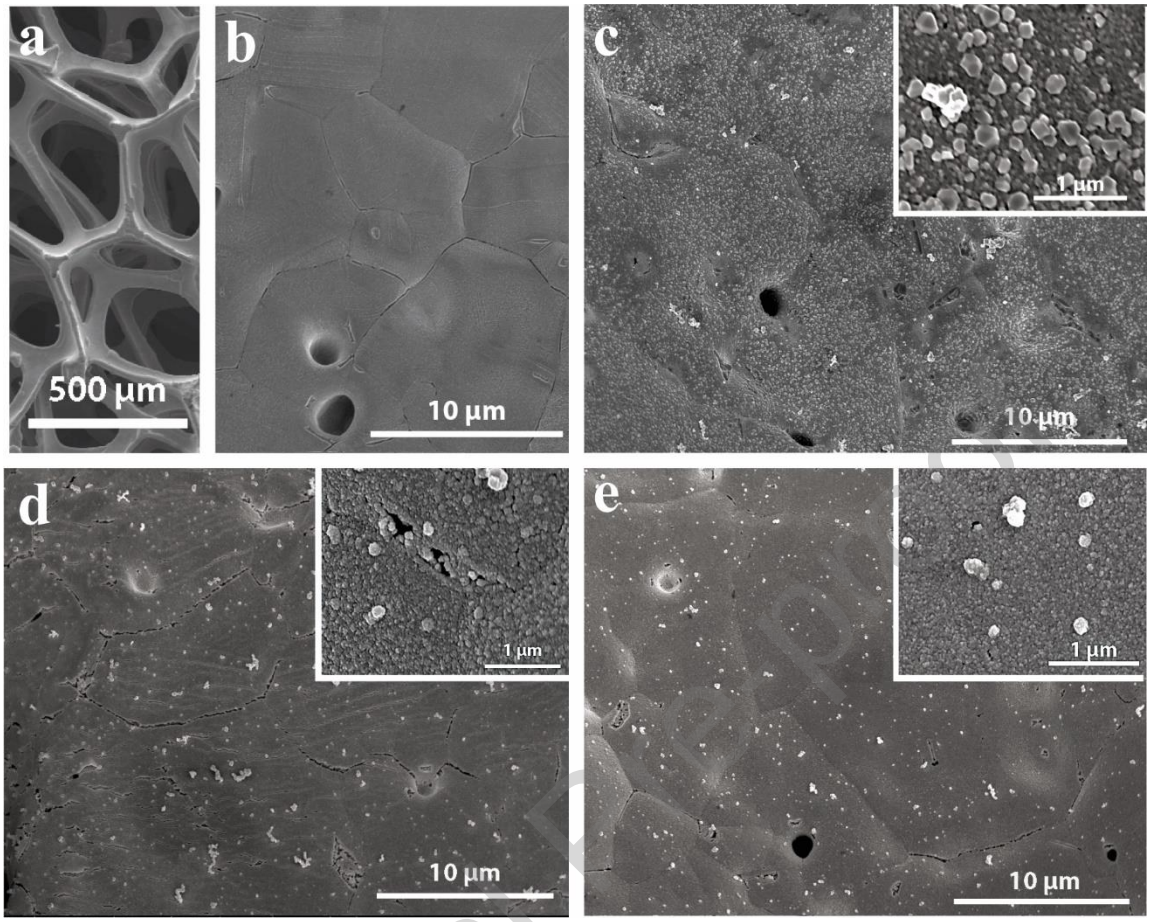

Figure 2. SEM images for (a) Cu foam at 65x; and (b) Cu foam, (c) Cu-Pt 60 s, (d) Cu-Pt 120 s and (e) Cu-Pt 180 s at 8 000x. Inset: Images taken at 50 000x.

Table 1. Elemental analysis data given from EDS spectra for different electrodes

Element	Composition (wt%)			
	Cu foam	**Cu-Pt 60 s**	**Cu-Pt 120 s**	**Cu-Pt 180 s**
Cu	98.76	91.63	80.2	81.19
O	1.24	2.40	6.25	1.75
Pt	-	5.97	13.54	17.06

3.2 Evaluating electrocatalytic properties for nitrate reduction by voltammetry

Capacitance analysis of Cu-Pt electrodes prepared at different Pt loadings controlled by electrodeposition time were evaluated in 0.1 Na_2SO_4. The increase of electroactive surface due to Pt

electrodeposition was proved by capacitance values of 0.66, 1.27, 1.59 and 1.84 F g^{-1} since higher electroactive surface present higher capacitance. Electrochemical nitrate reduction analyses of three-dimensional electrodes were recorded using CV in the potential range from 0.6 V to -0.4 V vs RHE at scan rate of 10 mV s^{-1}. Fig. 3a shows the cyclic voltammetry of copper foam in 0.1 Na_2SO_4 without (dotted line) and with 10 mmol L^{-1} $NaNO_3$ (solid line). It can be clearly observed the presence of an oxidation peak and shoulder, followed by two reduction peaks. When CV was conducted in presence of nitrate it was observed a dramatic increase on current response before the onset potential of hydrogen evolution associated to the nitrate reduction [40]. The oxidation (O_1) and reduction (R_1 and R_2) peaks were observed in presence of both electrolytes. However, to ensure that oxidation (O_1) and reduction (R_1 and R_2) peaks were not associated with nitrate, different concentrations of $NaNO_3$ (5, 10, 20 and 50 mmol L^{-1}) were added to the system and evaluated in the same potential range at scan rate of 10 mV s^{-1} (Fig. 3b). Despite the increase on nitrate concentrations the current peaks did not show notorious differences and seemed to be related to an electrode surface process and not to charge transfer processes with nitrate. These peaks have been previously associated to copper oxidation and copper reduction according to Eqs. (18) – (20).

$$O_1\colon\ 2Cu^0 + H_2O \rightarrow Cu_2O + 2H^+ + 2e^- \qquad E = 0.39\ V\ vs\ RHE \tag{18}$$

$$R_1\colon Cu^{1+} + 1e^- \rightarrow\ Cu^0 \qquad E = 0.44\ V\ vs\ RHE \tag{19}$$

$$R_2\colon Cu^{2+} + 2e^- \rightarrow\ Cu^0 \qquad E = 0.05\ V\ vs\ RHE \tag{20}$$

Fig. 3b illustrates how the increase on nitrate concentration results in a higher cathodic current and a displacement of the onset potential to more positive values. This result is indicative that nitrate reduction occurs at this range of negative potential closely overlapped with hydrogen evolution reaction (HER).

Linear sweep voltammetry (LSV) was conducted to further understand the cathodic process taking place at highly negative potentials to elucidate the different reduction processes taking place. Thus, LSV was recorded from 0.60 V to -1.4 V vs RHE at 10 mV s^{-1} to obtain a wide range of reduction of copper foam (Fig. 3c), similar experiment was performed for Cu-Pt 180 s (Fig. SM3). The electrochemical

behavior recorded in 0.1 mol L^{-1} Na_2SO_4 showed the hydrogen evolution reaction. Then, when 10 mmol L^{-1} $NaNO_3$ was added, two new reduction peaks were clearly detected. These two peaks can be associated to nitrate and nitrite reduction. To clearly identify the reduction reaction taking place at each peak potential, the LSV was recorded in 10 mmol L^{-1} $NaNO_2$. The LSV in presence of only NO_2^- illustrates a single peak located at -0.90 V vs RHE. Therefore, the nitrate reduction was located at -0.4 V vs RHE (Eq. 21) and nitrite reduction at -0.90 V vs RHE (Eq. 22) that was proved in potentiostatic experiment Fig. SM4 [36]. For Cu-Pt electrodes the reduction peaks were overlapped by HER and hard to differentiate (see Fig. SM3).

$$R_{NO_3^-}:\ {NO_3}^- + 2H^+ + 2e^- \rightarrow NO_2^- + H_2O \qquad E = -0.40\ V\ vs\ RHE \tag{21}$$

$$R_{NO_2^-}:\ NO_{2\,(ads)}^- + 7H^+ + 6e^- \longrightarrow NH_3 + 2H_2O \qquad E = -0.90\ V\ vs\ RHE \tag{22}$$

Fig. 3d shows the comparative CV analysis for the Cu-Pt nanocomposite foam electrodes in 0.1 mol L^{-1} Na_2SO_4 without (dotted line) and with 10 mmol L^{-1} $NaNO_3$ (solid line). The presence of Pt enhances HER that occurs at lower potentials of -0.18 V vs RHE than the -0.40 V vs RHE reported for pristine Cu foam. In presence of nitrate, the peaks O_1, R_1 and R_2 maintain their potential values as characteristic for copper [41]. Meanwhile, it is observed an increase in current response at -0.18 V vs RHE due to the coexistence of ERN and HER reactions in that region of potential.

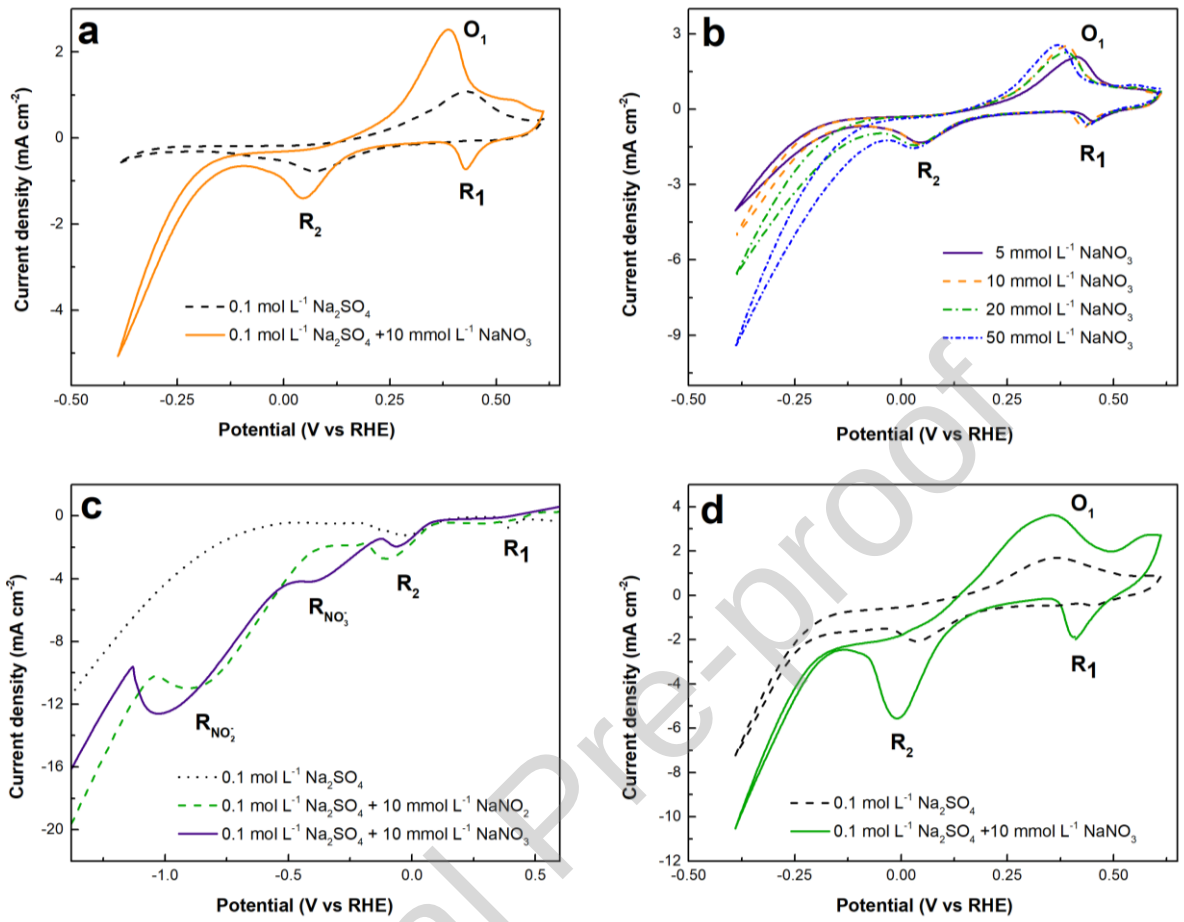

Figure 3. Cyclic voltammetry at 10 mV s^{-1} of (a) copper foam in absence and presence of $NaNO_3$, (b) copper foam with different concentrations of $NaNO_3$, and (c) Linear Sweep Voltammetry at 10 mV s^{-1} of copper foam in Na_2SO_4, $NaNO_3$ and $NaNO_2$ in the range of 0.6 V to -1.4 V vs RHE. (d) Cyclic voltammetry at 10 mV s^{-1} of Cu-Pt 180s electrode in absence and presence of $NaNO_3$.

3.3 Understanding enhanced electrochemical reduction of nitrate by Cu-Pt foam three-dimensional nanocomposite electrodes

Electrolytic treatment of nitrate solutions was conducted to benchmark the performance of Cu and Cu-Pt nano-enabled foams under comparable conditions. Fig. 4a shows that nano-enabling copper foam with Pt electrodeposited nanoparticles boosted the catalytic activity reaching almost complete reduction of nitrate in 120 min, while bare copper foam only attained 55% removal. Indeed, optimized Cu-Pt

composition shows a drastic acceleration of nitrate reduction kinetics by 4-fold from k_1=1.29×10^{-4} s^{-1} (R^2=0.932) for Cu foam up to k_1=4.03×10^{-4} s^{-1} (R^2=0.998) for Cu-Pt 180 s (Table 2). To understand how nanoparticles affect the electrocatalytic reduction of nitrate, a blank experiment using electrodeposited Cu nanoparticles (180s) on Cu foam was performed. After 120 min, ~57% of nitrate reduction was achieved. These results allow inferring that there is no significant impact of surface area increase by the addition of nanoparticles on ERN; however, it occurs the synergistic role of bimetallic catalytic sites on the electrochemically driven reduction of nitrate.

Fig. 4a shows a notorious change on the nitrate removal profile after 15 min of electrolysis when comparing pristine Cu foam with Pt nano-enabled Cu foam. All the electrodes had an analogous gradual NO_3^--N conversion (~ 27-35 %) until the first 15 min of electrolysis. After that time, it was possible to observe that by increasing the Pt electrodeposition time from 0 s to 180 s, the NO_3^--N conversion gradually increased from 55% for Cu to 80% for Cu-Pt 60 s, 88% for Cu-Pt 120 s, and 94% for Cu-Pt 180 s. However, further increase on Pt loading resulted in a loss of performance attaining solely 80% for Pt-Cu 360 s. The differentiated behavior can be associated to the different role of electrocatalytic metals in the composite and the conversion at the bimetallic catalytic centers. Copper is an electrocatalyst with excellent capabilities to reduce nitrate to nitrite [40,42,43]. The first reduction following reaction (2) is themed as the limiting step of the overall process in electrochemical systems [24]. This faster reduction to nitrite has been explained by two factors promoted by copper: (i) the ease adsorption of nitrate on copper surface that facilitates the inner-sphere reduction process, and (ii) the fast charge injection in nitrate facilitated by copper electrocatalytic sites. The reduction of nitrate to nitrite is fundamentally driven by an electrochemical-chemical-electrochemical (ECE) mechanism (Reactions 2 - 4). The first electron transfer yields a short lived (~20 μs) nitrate di-anion radical (NO_3^{2-}) [44], which is an unfavored process given the high energy of the lowest unoccupied molecular π* orbital (LUMO π*) of nitrate. Thus, the reduction of nitrate to nitrite is considered a sluggish reaction. Metals with highly occupied d-orbitals and unclosed d-orbital shells (*i.e.*, copper) have been identified as ideal given their energy levels similar to nitrate's LUMO π* facilitating charge transfer processes [24,45]. Some groups have reported cathodic passivation

of copper electrodes over time decreasing reduction efficiency, probably associated to the formation of copper oxides [46]. This would explain the kinetics deceleration observed in Fig. 4a after 15 min electrolysis for pristine copper foam and not observed for Cu-Pt electrodes. Nano-decoration of Cu foam with Pt opens alternative reduction mechanisms that can synergistically enhance reduction of nitrate as corroborated experimentally. Platinum incorporation displaces the hydrogen evolution onset potential (cf. Fig. 3d) yielding $H_{(ad)}$ from reaction (5) and evolving hydrogen at the cathode by reaction (23).

$$2H_2O + 2e^- \longrightarrow H_2 + 2OH^- \quad (23)$$

Hydrogen generation can contribute to the reduction process through catalytic hydrogenation mechanisms. Hydrogen gas (H_2) follows dissociative adsorption on platinoid metals (*i.e.,* Pt) yielding reactive adsorbed atoms of $H_{(ad)}$ that have high reduction potential. The $H_{(ad)}$ enables an indirect electrochemical reduction mechanism that can enact nitrate reduction kinetics in the following ways. First, neighboring $H_{(ad)}$ close to copper atoms can reduce oxidized metal (*i.e.*, Cu_2O, and CuO) to Cu^0 following a hydrogen spill-over reaction. This reaction regenerates the copper catalytic center enabling faster nitrate reduction, as can be deduced from the trends of Fig. 4a and the higher accumulation of nitrite by-product seen in Fig. 4b. In the case of the experiments using Cu-Pt electrodes, the maximum amount of [NO_2^--N] was between 2.0 x to 2.4 x higher than the bare Cu. Second, nitrite hydrogenation reactions catalyzed by platinum are known to be extremely fast and efficient despite of being uncapable of reducing nitrate [36,47–49]. This effect is illustrated by the nitrite concentration profile of Fig. 4b. Note that pristine Cu foam electrode attained a pseudo-constant concentration of nitrite in solution that origins from the balanced continuous generation of nitrite from nitrate reduction following reaction (21), and nitrite reduction to ammonia according to reaction (22). The synergistic effect of the coexistence between hydrogen and electrocatalysis is defined by the Pt loading on the copper foam. When a certain amount of the Pt electrodeposited is surpassed, as in the case of Cu-Pt 360 s, a reverse trend in the NO_3^--N conversion was detected. Indeed, the nitrate decay was quite like the one observed for Cu-Pt 60 s. This means that with higher times of electrodeposition that result in higher Pt loading, the formation of bigger Pt clusters may have a detrimental effect. Excess of Pt coverage decreases the electroreduction kinetic

rate of nitrate conversion. This behavior is confirmed by the pseudo-first order kinetic constants, which increased from k_1=1.29×10^{-4} s^{-1} (R^2=0.932) Cu foam to k_1=4.03×10^{-4} s^{-1} (R^2=0.998) Cu-Pt 180 s but decreased to k_1=2.35×10^{-4} s^{-1} (R^2=0.989) when using the Cu-Pt 360 s (Table2).

Electrogeneration of ammonia (Fig. 4c and Table 2) was enhanced 2.0 times from pristine Cu (97.5 mg NH_3-N L^{-1} g_{cat}^{-1}) to Cu-Pt 180 s (194.4 mg NH_3-N L^{-1} g_{cat}^{-1}). As observed for the other N-species, the generation of [NH_3-N] decreased for the experiment using Cu-Pt 360s following a similar trend to Cu-Pt 60 s, achieving final [NH_3-N] values around 126.3 – 128.9 mg NH_3-N L^{-1} g_{cat}^{-1}. The amount of the [NH_3-N] reaction product differs depending on the Pt loadings. At higher nitrate conversions, [NH_3-N] selectivity increased, suggesting that nitrite hydrogenation occurred. Under aqueous and room temperature conditions, H_2 would tend to adsorb in a dissociate way on Pt to form H atoms and convert NO_2^- to NH_3 [39].

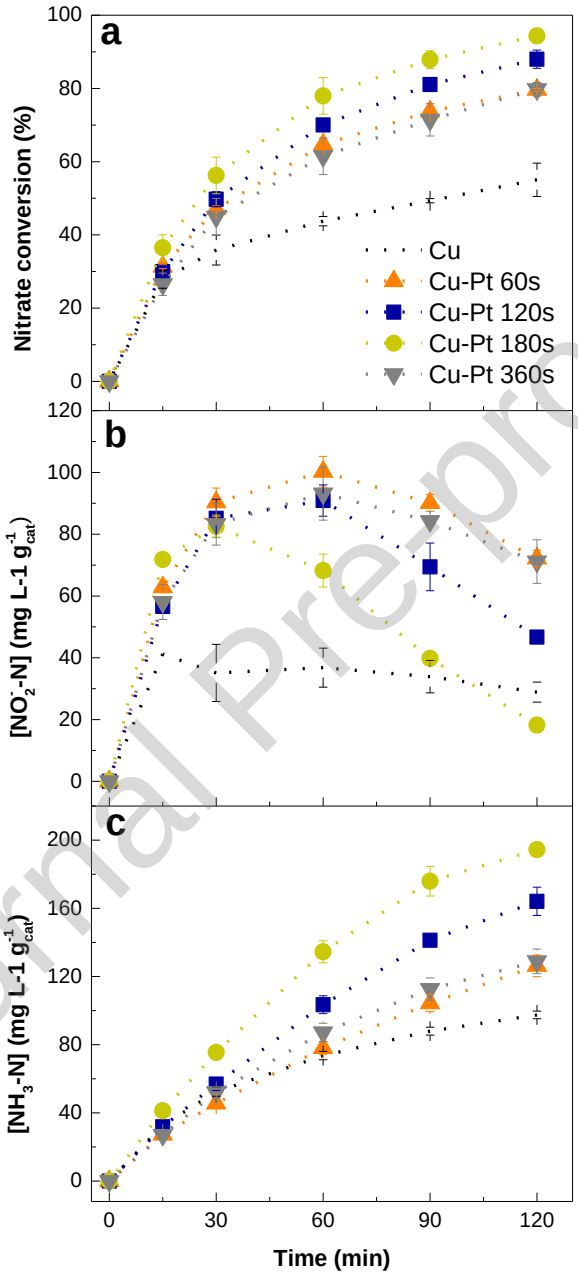

Figure 4. (a) [NO_3^--N] conversion, (b) [NO_2^--N] and (c) [NH_3-N] evolutions over time for the electroreduction of 30 mg L^{-1} NO_3^--N in 12.5 mmol L^{-1} Na_2SO_4 at 0.09 A, using (◇) Cu foam, (▲) Cu-Pt 60 s, (■) Cu-Pt 120 s, (●) Cu-Pt 180 s and (▼) Cu-Pt 360 s, as cathodic materials.

Table 2. Key fitted and calculated parameters from the ERN experiments 30 mg L^{-1} NO_3^--N in 12.5 mmol L^{-1} Na_2SO_4 at 0.09 A during 120 min of treatment time.

Electrode	E_{cell} (V)	$k_1 \times 10^{-4}$ (s^{-1})	Nitrate conversion (%)	NH_3-N (mg L^{-1} g_{cat}^{-1})
Cu foam	9.4 ± 0.8	1.29 ± 0.05	55 ± 4	97.5 ± 2.2
Cu-Pt 60 s	8.4 ± 1.7	2.44 ± 0.01	80 ± 1	126.3 ± 6.2
Cu-Pt 120 s	8.7 ± 1.9	3.08 ± 0.16	88 ± 3	164.1 ± 8.1
Cu-Pt 180 s	8.8 ± 0.2	4.03 ± 0.51	94 ± 2	194.4 ± 3.6
Cu-Pt 360 s	9.9 ± 0.1	2.35 ± 0.23	80 ± 2	128.9 ± 6.4

According to Fig. 5a, the Faradaic efficiency (FE) associated to NH_3 production varied between 11 to 22%. The lowest value corresponded to the efficiency with which electrons attained NH_3 using pristine Cu, while the two-fold higher FE corresponded to Cu-Pt 180 s. These FE values may be related to the competition reactions that occur during the treatment process, as is the case of HER previously described. The FE agrees with ammonia productivity that achieved a maximum value of 194.4 mg NH_3-N L^{-1} g_{cat}^{-1} for Cu-Pt 180 s. The representation of ammonia selectivity (S_{NH_3}) respect to Pt loading illustrates a volcano plot that allows clearly identifying the optimum composition for the nano-composite three-dimensional electrodes (Fig. 5b). A maximum of 84% of selectivity towards NH_3 using 0.36 wt% Pt was obtained for Cu-Pt 180 s. It is important to remark that these nanocomposite electrodes containing lower amounts of Pt (< 0.50 wt%) lead to competitive selectivity for resource recovery and fast kinetic rate constants of nitrate abatement for water remediation.

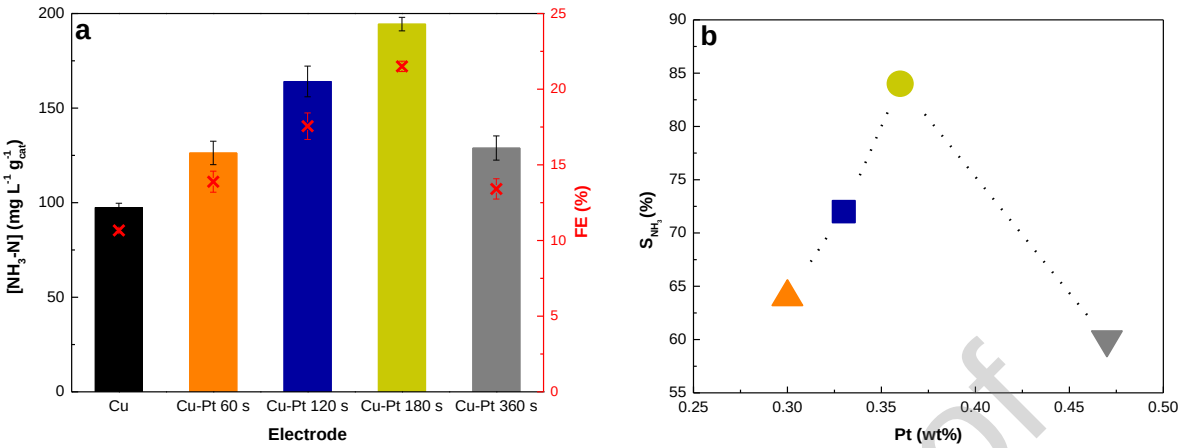

Figure 5. (a) **A**mount of NH_3-N electrogenerated by mass of electrocatalyst used (bars) and Faradaic efficiency (red crosses) for **Cu foam**, **Cu-Pt 60 s**, **Cu-Pt 120 s**, **Cu-Pt 180 s** and **Cu-Pt 360 s** and (b) selectivity towards ammonia for the different Pt loadings ((▲) Cu-Pt 60 s, (■) Cu-Pt 120 s, (●) Cu-Pt 180 s and (▼) Cu-Pt 360 s). Results at the end of the treatment time (120 min).

Another essential engineering figure of merit is the electric energy per order (EE/O), which evaluates the energy necessary to decrease the concentration of NO_3^--N one order of magnitude (kWh m^{-3} $order^{-1}$). According to Fig. 6, the values of the EE/O ranged between 13 and 42 kWh m^{-3} $order^{-1}$. The lowest and highest EE/O values corresponded to the experiment with Cu-Pt 180 s and Cu foam, respectively. These EE/O results reflect the balance between the nitrate reduction kinetics rate (k_1, Table 2) and the cell potential (E_{cell}, Fig. 6) during the treatment. This means that materials with higher k_1 and lower E_{cell} may attain the lowest EE/O. Therefore, Cu-Pt 180 s seems to be a promising electrocatalytic material for the ERN due to the synergetic effect between Cu and the Pt nano-decoration. The minimization of Pt usage can decrease the capital cost of these bimetallic electrode. Furthermore, the electrodeposition method allows a stable modification by the direct growth of nanostructures strongly attached on the copper substrate. The evaluation of Cu-Pt 180 s leaching under accelerated aging conditions (Figure SM5) shows a not detectable Cu dissolution and low amount of platinum 0.159 μg L^{-1} indicating a high stability of the

bimetallic electrode. This new procedure can provide a new framework for selective nitrate reduction treatment and resource recovery technologies.

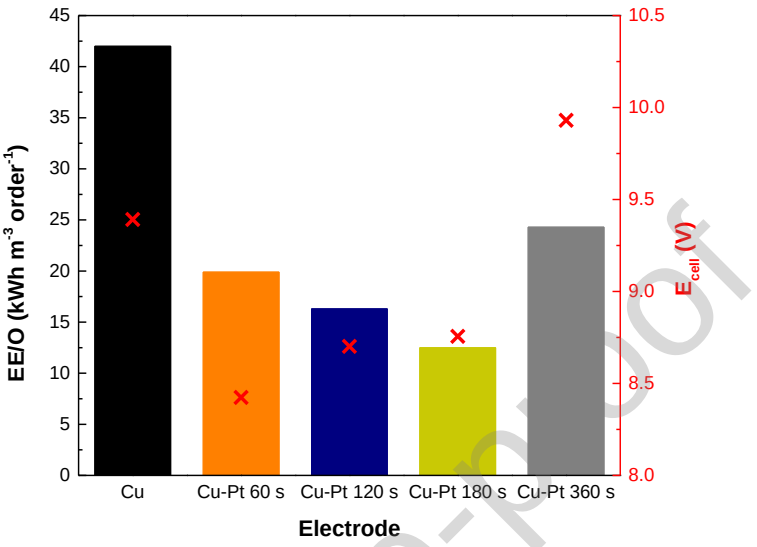

Figure 6. Energy consumption per order after 360 min (bars) and cell potential average (red crosses) for the electroreduction of 30 mg L^{-1} NO_3^--N in 12.5 mmol L^{-1} Na_2SO_4 at 0.09 A, using **Cu foam**, **Cu-Pt 60 s**, **Cu-Pt 120 s**, **Cu-Pt 180 s** and **Cu-Pt 360 s**, as cathodic materials.

4. Conclusions

Bimetallic Cu-Pt electrodes were synthesized by electrodeposition with different amounts of Pt controlled by time. Platinum nanoparticles growth on the surface of copper foam changed the electrocatalytic response of electrodes, mainly by the synergistic effects induced by Cu-Pt nanointerfaces that enable hybridized mechanisms of catalytic electrochemical and hydrogenation reduction processes. These new bimetallic active catalytic sites present a higher nitrate conversion than monometallic copper electrode by overcoming the limiting step related with nitrate to nitrite initial reduction reaction. While copper surface promotes the reduction of nitrate to nitrite, platinum nanoparticles boost the conversion of nitrite to ammonia. The copper foam electrode presents 55% of nitrate conversion while Cu-Pt electrodes shows higher nitrate conversion. Under comparable operating conditions, the different Pt loadings (~0.30

wt%, ~0.33 wt%, ~0.36 wt%, ~0.47 wt% electrodeposited at 60 s, 120 s, 180 s and 360 s, respectively) on Cu foam were able to elevate nitrate conversion. Cu-Pt 180 s presented almost total nitrate conversion (~94%), k_1 = 4.03 x10^{-4} s^{-1}, 194.4 mg NH_3-N L^{-1} g_{cat}^{-1}, S_{NH_3} = 84% and FE = 22% in 120 min. This is an improvement respect previous reports in literature when benchmarking different electrocatalytic materials (Table SM1). On the other hand, higher loadings of platinum (360 s) in the nanocomposite induced inhibition of the reduction process due to the loss of the synergistic interaction between Cu-Pt sites.

The lowest value of electrical energy per order was 13 kWh m^{-3} $order^{-1}$ for the Cu-Pt 180 s, suggesting that this is an ideal quantity of platinum on the copper foam surface. These results highlight the potential of Cu-Pt electrodes to treat contaminated water streams containing nitrate, while providing a unique opportunity for circular economy by enabling decentralized ammonia recovery from polluted water sources. Ammonia recovery from nitrate polluted water can become an opportunity for agricultural sustainable production.

Acknowledgments

The authors acknowledge the support of the Centre National de la Recherche Scientifique (CNRS). This work was partially funded by the National Science Foundation (NSF) through the Nanosystems Engineering Research Center for Nanotechnology-Enabled Water Treatment under project EEC-1449500. This project has received funding from the European Union's Horizon 2020 research and innovation program under the Marie Skłodowska-Curie grant agreement No 843870. We would like to thank Kenneth R. Flores for his assistance on the ICP-MS measurements. We thank De Nora Tech, LLC for kindly providing the DSA® electrodes used as anode in our electrochemical system. We acknowledge the use of facilities within the Eyring Materials Center at Arizona State University supported in part by NNCI-ECCS-1542160.

References

[1] D. Zhou, R. Zhou, R. Zhou, B. Liu, T. Zhang, Y. Xian, P.J. Cullen, X. Lu, K. (Ken) Ostrikov, Sustainable ammonia production by non-thermal plasmas: Status, mechanisms, and opportunities, Chem. Eng. J. 421 (2021) 129544. https://doi.org/10.1016/j.cej.2021.129544.

[2] C. Tang, S.Z. Qiao, How to explore ambient electrocatalytic nitrogen reduction reliably and insightfully, Chem. Soc. Rev. 48 (2019) 3166–3180. https://doi.org/10.1039/c9cs00280d.

[3] M.R. Burkart, J.D. Stoner, Nitrate in aquifers beneath agricultural systems, Water Sci. Technol. 56 (2007) 59–69. https://doi.org/10.2166/wst.2007.436.

[4] A. Menció, J. Mas-Pla, N. Otero, O. Regàs, M. Boy-Roura, R. Puig, J. Bach, C. Domènech, M. Zamorano, D. Brusi, A. Folch, Nitrate pollution of groundwater; all right. . ., but nothing else?, Sci. Total Environ. 539 (2016) 241–251. https://doi.org/10.1016/j.scitotenv.2015.08.151.

[5] Y.Y. Yang, G.S. Toor, Sources and mechanisms of nitrate and orthophosphate transport in urban stormwater runoff from residential catchments, Water Res. 112 (2017) 176–184. https://doi.org/10.1016/j.watres.2017.01.039.

[6] M.G. Rupert, Decadal-Scale Changes of Nitrate in Ground Water of the United States, 1988-2004,

J. Environ. Qual. 37 (2008) S-240-S-248. https://doi.org/10.2134/jeq2007.0055.

[7] K.R. Burow, B.T. Nolan, M.G. Rupert, N.M. Dubrovsky, Nitrate in groundwater of the United States, 1991-2003, Environ. Sci. Technol. 44 (2010) 4988–4997. https://doi.org/10.1021/es100546y.

[8] X. Wang, M. Zhu, G. Zeng, X. Liu, C. Fang, C. Li, A three-dimensional Cu nanobelt cathode for highly efficient electrocatalytic nitrate reduction, Nanoscale. 12 (2020) 9385–9391. https://doi.org/10.1039/c9nr10743f.

[9] Y. Wang, W. Zhou, R. Jia, Y. Yu, B. Zhang, Unveiling the Activity Origin of a Copper-based Electrocatalyst for Selective Nitrate Reduction to Ammonia, Angew. Chemie - Int. Ed. 59 (2020) 5350–5354. https://doi.org/10.1002/anie.201915992.

[10] WHO, Nitrate and nitrite in drinking-water, 2016. https://www.who.int/water_sanitation_health/dwq/chemicals/nitrate-nitrite-background-jan17.pdf?ua=1.

[11] EPA, National primary drinking water regulations, 2017. https://www.epa.gov/ground-water-and-drinking-water/national-primary-drinking-water-regulations.

[12] A.H. Wolfe, J.A. Patz, Reactive nitrogen and human health: Acute and long-term implications, Ambio. 31 (2002) 120–125. https://doi.org/10.1579/0044-7447-31.2.120.

[13] R.R. Jones, P.J. Weyer, C.T. Dellavalle, M. Inoue-Choi, K.E. Anderson, K.P. Cantor, S. Krasner, K. Robien, L.E. Beane Freeman, D.T. Silverman, M.H. Ward, Nitrate from drinking water and diet and bladder cancer among postmenopausal women in Iowa, Environ. Health Perspect. 124 (2016) 1751–1758. https://doi.org/10.1289/EHP191.

[14] J. Schullehner, B. Hansen, M. Thygesen, C.B. Pedersen, T. Sigsgaard, Nitrate in drinking water and colorectal cancer risk: A nationwide population-based cohort study, Int. J. Cancer. 143 (2018) 73–79. https://doi.org/10.1002/ijc.31306.

[15] A. Temkin, S. Evans, T. Manidis, C. Campbell, O. V. Naidenko, Exposure-based assessment and economic valuation of adverse birth outcomes and cancer risk due to nitrate in United States

drinking water., Environ. Res. 176 (2019) 108442. https://doi.org/10.1016/j.envres.2019.04.009.

[16] C.J.M. Van Der Ham, M.T.M. Koper, D.G.H. Hetterscheid, Challenges in reduction of dinitrogen by proton and electron transfer, Chem. Soc. Rev. 43 (2014) 5183–5191. https://doi.org/10.1039/c4cs00085d.

[17] A.R. Singh, B.A. Rohr, J.A. Schwalbe, M. Cargnello, K. Chan, T.F. Jaramillo, I. Chorkendorff, J.K. Nørskov, Electrochemical Ammonia Synthesis - The Selectivity Challenge, ACS Catal. 7 (2017) 706–709. https://doi.org/10.1021/acscatal.6b03035.

[18] M.A. Shipman, M.D. Symes, Recent progress towards the electrosynthesis of ammonia from sustainable resources, Catal. Today. 286 (2017) 57–68. https://doi.org/10.1016/j.cattod.2016.05.008.

[19] V. Kyriakou, I. Garagounis, E. Vasileiou, A. Vourros, M. Stoukides, Progress in the Electrochemical Synthesis of Ammonia, Catal. Today. 286 (2017) 2–13. https://doi.org/10.1016/j.cattod.2016.06.014.

[20] I. Katsounaros, On the assessment of electrocatalysts for nitrate reduction, Curr. Opin. Electrochem. 28 (2021) 100721. https://doi.org/10.1016/j.coelec.2021.100721.

[21] D. Hao, Z. gang Chen, M. Figiela, I. Stepniak, W. Wei, B.J. Ni, Emerging alternative for artificial ammonia synthesis through catalytic nitrate reduction, J. Mater. Sci. Technol. 77 (2021) 163–168. https://doi.org/10.1016/j.jmst.2020.10.056.

[22] P.H. van Langevelde, I. Katsounaros, M.T.M. Koper, Electrocatalytic Nitrate Reduction for Sustainable Ammonia Production, Joule. 5 (2021) 290–294. https://doi.org/10.1016/j.joule.2020.12.025.

[23] M. Marcos-Hernández, G. Antonio Cerrón-Calle, Y. Ge, S. Garcia-Segura, C.M. Sánchez-Sánchez, A.S. Fajardo, D. Villagrán, Effect of surface functionalization of Fe3O4 nano-enabled electrodes on the electrochemical reduction of nitrate, Sep. Purif. Technol. (2021) 119771. https://doi.org/10.1016/j.seppur.2021.119771.

[24] S. Garcia-Segura, M. Lanzarini-Lopes, K. Hristovski, P. Westerhoff, Electrocatalytic reduction of

nitrate: Fundamentals to full-scale water treatment applications, Appl. Catal. B Environ. 236 (2018) 546–568. https://doi.org/10.1016/j.apcatb.2018.05.041.

[25] C. Lu, X. Lu, K. Yang, H. Song, S. Zhang, A. Li, Cu, Ni and multi-walled carbon-nanotube-modified graphite felt electrode for nitrate electroreduction in water, J. Mater. Sci. 56 (2021) 7357–7371. https://doi.org/10.1007/s10853-020-05764-3.

[26] A.S. Fajardo, P. Westerhoff, C.M. Sanchez-Sanchez, S. Garcia-Segura, Earth-abundant elements a sustainable solution for electrocatalytic reduction of nitrate, Appl. Catal. B Environ. 281 (2021) 119465. https://doi.org/10.1016/j.apcatb.2020.119465.

[27] S.L. Foster, S.I.P. Bakovic, R.D. Duda, S. Maheshwari, R.D. Milton, S.D. Minteer, M.J. Janik, J.N. Renner, L.F. Greenlee, Catalysts for nitrogen reduction to ammonia, Nat. Catal. 1 (2018) 490–500. https://doi.org/10.1038/s41929-018-0092-7.

[28] J. Martínez, A. Ortiz, I. Ortiz, State-of-the-art and perspectives of the catalytic and electrocatalytic reduction of aqueous nitrates, Appl. Catal. B Environ. 207 (2017) 42–59. https://doi.org/10.1016/j.apcatb.2017.02.016.

[29] C.M. Sánchez-Sánchez, J. Solla-Gullón, F.J. Vidal-Iglesias, A. Aldaz, V. Montiel, E. Herrero, Imaging structure sensitive catalysis on different shape-controlled platinum nanoparticles, J. Am. Chem. Soc. 132 (2010) 5622–5624. https://doi.org/10.1021/ja100922h.

[30] M.A. Montiel, J. Solla-Gullón, C.M. Sánchez-Sánchez, Electrochemical reactivity and stability of platinum nanoparticles in imidazolium-based ionic liquids, J. Solid State Electrochem. 20 (2016) 1043–1052. https://doi.org/10.1007/s10008-015-3014-5.

[31] J. V. Perales-Rondón, E. Herrero, J. Solla-Gullón, C.M. Sánchez-Sánchez, V. Vivier, Oxygen crossover effect on palladium and platinum based electrocatalysts during formic acid oxidation studied by scanning electrochemical microscopy, J. Electroanal. Chem. 793 (2017) 218–225. https://doi.org/10.1016/j.jelechem.2016.12.049.

[32] L. Zhang, J. Perales-Rondón, A. Thomère, J. Blanchard, C. Sánchez-Sánchez, Platinum-zeolite hybrid catalyst for the electrooxidation of formic acid, J. Electroanal. Chem. In pess (2021)

115491. https://doi.org/10.1016/j.jelechem.2021.115491.

[33] Y.B. Yin, S. Guo, K.N. Heck, C.A. Clark, C.L. Coonrod, M.S. Wong, Treating Water by Degrading Oxyanions Using Metallic Nanostructures, ACS Sustain. Chem. Eng. 6 (2018) 11160–11175. https://doi.org/10.1021/acssuschemeng.8b02070.

[34] K.N. Heck, S. Garcia-Segura, P. Westerhoff, M.S. Wong, Catalytic Converters for Water Treatment, Acc. Chem. Res. 52 (2019) 906–915. https://doi.org/10.1021/acs.accounts.8b00642.

[35] M.A. Hasnat, M.A. Rashed, S. Ben Aoun, S.M.N. Uddin, M. Saiful Alam, S. Amertharaj, R.K. Majumder, N. Mohamed, Dissimilar catalytic trails of nitrate reduction on Cu-modified Pt surface immobilized on H+ conducting solid polymer, J. Mol. Catal. A Chem. 383–384 (2014) 243–248. https://doi.org/10.1016/j.molcata.2013.12.015.

[36] M.A. Hasnat, S. Ben Aoun, S.M. Nizam Uddin, M.M. Alam, P.P. Koay, S. Amertharaj, M.A. Rashed, M.M. Rahman, N. Mohamed, Copper-immobilized platinum electrocatalyst for the effective reduction of nitrate in a low conductive medium: Mechanism, adsorption thermodynamics and stability, Appl. Catal. A Gen. 478 (2014) 259–266. https://doi.org/10.1016/j.apcata.2014.04.017.

[37] N. Lotfi, T. Shahrabi, Y. Yaghoubinezhad, G.B. Darband, Direct electrodeposition of platinum nanoparticles@graphene oxide@nickel-copper@nickel foam electrode as a durable and cost-effective catalyst with remarkable performance for electrochemical hydrogen evolution reaction, Appl. Surf. Sci. 505 (2020). https://doi.org/10.1016/j.apsusc.2019.144571.

[38] P. Zhu, Y. Zhao, Cyclic voltammetry measurements of electroactive surface area of porous nickel: Peak current and peak charge methods and diffusion layer effect, Mater. Chem. Phys. 233 (2019) 60–67. https://doi.org/10.1016/j.matchemphys.2019.05.034.

[39] K.N. Heck, S. Garcia-Segura, P. Westerhoff, M.S. Wong, Catalytic Converters for Water Treatment, Acc. Chem. Res. 52 (2019) 906–915. https://doi.org/10.1021/acs.accounts.8b00642.

[40] G.E. Dima, A.C.A. De Vooys, M.T.M. Koper, Electrocatalytic reduction of nitrate at low concentration on coinage and transition-metal electrodes in acid solutions, J. Electroanal. Chem.

554–555 (2003) 15–23. https://doi.org/10.1016/S0022-0728(02)01443-2.

[41] S.D. Giri, A. Sarkar, Electrochemical Study of Bulk and Monolayer Copper in Alkaline Solution, J. Electrochem. Soc. 163 (2016) H252–H259. https://doi.org/10.1149/2.0071605jes.

[42] K. Bouzek, M. Paidar, A. Sadílková, H. Bergmann, Electrochemical reduction of nitrate in weakly alkaline solutions, J. Appl. Electrochem. 31 (2001) 1185–1193. https://doi.org/10.1023/A:1012755222981.

[43] D. Reyter, D. Bélanger, L. Roué, Study of the electroreduction of nitrate on copper in alkaline solution, Electrochim. Acta. 53 (2008) 5977–5984. https://doi.org/10.1016/j.electacta.2008.03.048.

[44] A.R. Cook, N. Dimitrijevic, B.W. Dreyfus, D. Meisel, L.A. Curtiss, D.M. Camaioni, Reducing radicals in nitrate solutions. The NO32- system revisited, J. Phys. Chem. A. 105 (2001) 3658–3666. https://doi.org/10.1021/jp0038052.

[45] G.F. Chen, Y. Yuan, H. Jiang, S.Y. Ren, L.X. Ding, L. Ma, T. Wu, J. Lu, H. Wang, Electrochemical reduction of nitrate to ammonia via direct eight-electron transfer using a copper–molecular solid catalyst, Nat. Energy. 5 (2020) 605–613. https://doi.org/10.1038/s41560-020-0654-1.

[46] F. Epron, F. Gauthard, C. Pinéda, J. Barbier, Catalytic Reduction of Nitrate and Nitrite on Pt-Cu/Al2O3 Catalysts in Aqueous Solution: Role of the Interaction between Copper and Platinum in the Reaction, J. Catal. 198 (2001) 309–318. https://doi.org/10.1006/jcat.2000.3138.

[47] S. Kerkeni, E. Lamy-Pitara, J. Barbier, Copper-platinum catalysts prepared and characterized by electrochemical methods for the reduction of nitrate and nitrite, Catal. Today. 75 (2002) 35–42. https://doi.org/10.1016/S0920-5861(02)00041-X.

[48] F. Gauthard, F. Epron, J. Barbier, Palladium and platinum-based catalysts in the catalytic reduction of nitrate in water: Effect of copper, silver, or gold addition, J. Catal. 220 (2003) 182–191. https://doi.org/10.1016/S0021-9517(03)00252-5.

[49] A. Aristizábal, S. Contreras, N. Barrabés, J. Llorca, D. Tichit, F. Medina, Catalytic reduction of nitrates in water on Pt promoted Cu hydrotalcite-derived catalysts: Effect of the Pt-Cu alloy

formation, Appl. Catal. B Environ. 110 (2011) 58–70. https://doi.org/10.1016/j.apcatb.2011.08.024.

Graphical abstract

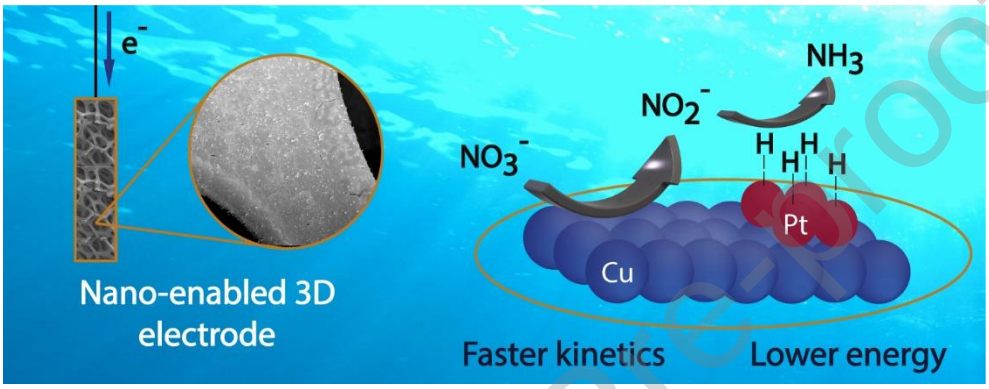

CREDIT STATEMENTM

Author Contributions: Conceptualization, G.A.C.-C., A.S.F., C.M.S.-S., S.G-S.; methodology, G.A.C.-C., A.S.F., C.M.S.-S., S.G-S.; validation, G.A.C.-C., A.S.F.; investigation, G.A.C.-C., A.S.F.; formal analysis, G.A.C.-C., A.S.F., C.M.S.-S., S.G-S.; data curation, G.A.C.-C., A.S.F.; resources, S.G.-S.; visualization, G.A.C.-C., A.S.F., C.M.S.-S., S.G-S.; writing—original draft G.A.C.-C., A.S.F., C.M.S.-S., S.G-S.; writing—review and editing, G.A.C.-C., A.S.F., C.M.S.-S., S.G-S.; supervision, C.M.S.-S., S.G-S.; project administration, S.G-S.; funding acquisition, A.S.F., C.M.S.-S., S.G-S. All authors read and approved the final manuscript.

Conflict of interest

Authors declare no conflict of interest.

Highlights

- Electrochemical reduction of nitrate (ERN) with sustainable ammonia recovery.
- Synthesizing bimetallic Cu-Pt foam electrodes by electrodeposition.
- Pt nano-decoration enables outer sphere hydrogenation reactions.
- Nano-enabled materials outperform pristine Cu foam in kinetics and NH_3 recovery.
- Cu-Pt (180 s) has the best NH_3 selectivity with low EE/O of 13 kWh m^{-3} $order^{-1}$.